# Complexes of Fe(III) and Ga(III) Derived from the Cyclic 6- and 7-Membered Hydroxamic Acids Found in Mixed Siderophores

Pawel Jewula, Mickaël Grandmougin, Mélanie Choppin, Anna Maria Chiara Tivelli, Agnese Amati, Yoann Rousselin, Lydia Karmazin, Jean-Claude Chambron, Michel Meyer

EurJIC
European Journal of Inorganic Chemistry

Research Article
doi.org/10.1002/ejic.202300038

Chemistry Europe
European Chemical Societies Publishing

www.eurjic.org

# Complexes of Fe(III) and Ga(III) Derived from the Cyclic 6- and 7-Membered Hydroxamic Acids Found in Mixed Siderophores

Pawel Jewula,[a] Mickaël Grandmougin,[a] Mélanie Choppin,[a] Anna Maria Chiara Tivelli,[a] Agnese Amati,[b] Yoann Rousselin,[a] Lydia Karmazin,[b] Jean-Claude Chambron,*[a, b] and Michel Meyer*[a]

Six- and seven-membered cyclic hydroxamic acids are found as terminal binding units in different families of siderophores, including exochelins and mycobactins. The simplest models of these preorganized chelating ligands were known, but their coordination chemistry with $Fe^{3+}$, the target metal ion of siderophores, had never been reported. Four complexes were synthesized and studied: two $Fe^{3+}$ complexes, one with the six-membered ring hydroxamate $PIPO^-$ and one with the seven-membered ring hydroxamate $AZEPO^-$, and the two corresponding $Ga^{3+}$ complexes. X-ray diffraction studies showed that the interligand repulsion energies were better minimized in the case of the $AZEPO^-$ complexes whatever the metal cation considered, and that the Fe–O bond distances were shorter in $[Fe(AZEPO)_3]$ by comparison with $[Fe(PIPO)_3]$.

## Introduction

Siderophores are secondary metabolites that are excreted by bacteria to (i) capture $Fe^{3+}$ in their environment from insoluble iron oxohydroxides, (ii) convey it across their membrane, and (iii) release it in the cytosol, where it is used for the synthesis of iron-based enzyme cofactors, such as iron-sulfur clusters or the heme.[1] Some siderophores have specialized functions. In mycobacteria, the extracellular hydrophilic exochelins and carboxymycobactins perform step (i) and subsequently deliver iron to the lipophilic mycobactins.[2] The latter are permanently located in the bacterial membrane, which allows them to carry out step (ii). Delivery of $Fe^{3+}$ to the cytosol usually proceeds through reduction to $Fe^{2+}$, but protonation of the Fe-siderophore complex has also been suggested as a possible mechanism.[3] Siderophores are interesting biological targets to fight against pathogenic bacteria, as the expression of those metabolites is related to the virulence of these microorganisms.[4] Siderophore-antibiotic conjugates have also been used in "Trojan horse" strategies.[5] From the chemical viewpoint, siderophores are $Fe^{3+}$-chelators. As $Fe^{3+}$ is a hard Lewis acid transition metal cation that forms preferably hexacoordinate complexes, siderophores often incorporate three oxygen-containing anionic bidentate chelating ligands, based mostly on the catecholate and/or the hydroxamate motif. Other oxygen-based chelating ligands found in siderophores are α-hydroxycarboxylates[6] and the deprotonated form of *N*-nitrosohydroxylamine, a unique motif found in Gramibactin.[7] More classical examples are enterobactin, a tripodal tris(catechol), for the former (Figure 1a), and desferriferrioxamine B (DFO), a linear tris(hydroxamic acid), for the latter (Figure 1b). Among the siderophores studied so far, enterobactin shows the highest binding constant for $Fe^{3+}$ ($K = 10^{49}$),

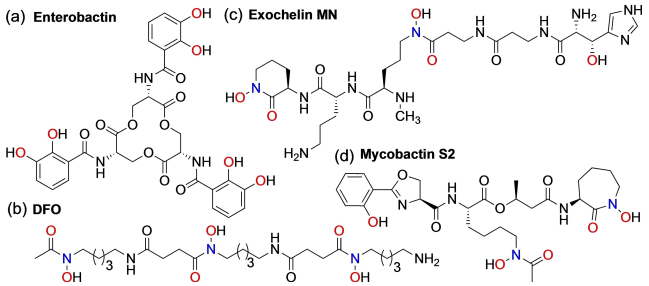


**Figure 1.** Examples of siderophores: (a) Catechol and (b) hydroxamic acid-based emblematic siderophores; (c) and (d) mixed siderophores containing a six-membered (c) and a seven-membered (d) cyclic hydroxamic acid. The coordinating oxygen atoms are highlighted in red.

[a] *Dr. P. Jewula, M. Grandmougin, M. Choppin, A. M. C. Tivelli, Dr. Y. Rousselin, Dr. J.-C. Chambron, Dr. M. Meyer*
*Institut de Chimie Moléculaire de l'Université de Bourgogne (ICMUB)*
*UMR 6302, CNRS*
*Université de Bourgogne*
*9 avenue Alain Savary, BP 47870*
*21078 Dijon Cedex (France)*
*E-mail: michel.meyer@u-bourgogne.fr*
http://www.icmub.com/
[b] *Dr. A. Amati, Dr. L. Karmazin, Dr. J.-C. Chambron*
*Institut de Chimie de Strasbourg*
*UMR 7177, CNRS*
*Université de Strasbourg*
*1 rue Blaise Pascal, BP 296 R 8*
*67008 Strasbourg Cedex (France)*
*E-mail: jcchambron@unistra.fr*
https://lclac.chimie.unistra.fr/

*Supporting information for this article is available on the WWW under https://doi.org/10.1002/ejic.202300038*

Research Article
doi.org/10.1002/ejic.202300038



outperforming desferriferrioxamine B by ca. 20 orders of magnitude.[1a] Enterobactin and desferriferrioxamine B differ by their topology, the number of anionic charges on the chelating subunits (2 vs. 1), and also by the fact that the catecholate ligand subunits of enterobactin are preorganized for chelation, whereas the linear hydroxamate motifs of desferriferrioxamine B, which preferentially adopt the *trans* conformation in the free state, are not.

There exists a third class of siderophores, the so-called mixed siderophores, which can incorporate up to three different metal-binding subunits. Whatever the topology (linear or branched), several representatives of this class show, as one of the terminal chelating subunits, a cyclic hydroxamic acid moiety, either six- (e.g. exochelin MN, Figure 1c)[8,9] or seven-membered (e.g. mycobactins, a member of this family of siderophores is shown in Figure 1d).[2b] These cyclic hydroxamic acid residues are attached to the rest of the chelator by an amide bond, the nitrogen atom substituting stereospecifically the carbon atom (3-C) α to the carbonyl function of the hydroxamic acid. The remarkable feature of the cyclic hydroxamates is that, as the catecholates, they are preorganized for chelation. We have discussed the consequences of this property in the case of the complexation of $UO_2^{2+}$.[10] The properties of the Fe(III) complexes of the simple model ligands catecholate ($CAT^{2-}$)[11] and *N*-methylhydroxamate ($NMA^-$)[12] (Figure 2) have been reported. This was not the case of the Fe(III) complexes of the models of the six-membered and seven-membered cyclic hydroxamic acids found in several siderophores, 1-hydroxy-2-piperidinone (PIPOH) and hexahydro-1-hydroxy-2H-azepin-2-one (AZEPOH), respectively, which were prepared and used for other purposes.[13,14] We have been interested for several years in the coordination chemistry of tetravalent cations of transition, lanthanide, and actinide metal families. These metal cations are Lewis-acidic, just as the ubiquitous $Fe^{3+}$ is, and a lead for the design and development of efficient chelators for these tetravalent cations is to get inspiration from the iron binding motifs found in siderophores.[1a] We reported a structural study of the complexes of deprotonated 1-hydroxy-2-piperidinone ($PIPO^-$) with tetravalent metal cations, including $Zr^{4+}$, $Hf^{4+}$, $Ce^{4+}$, $Th^{4+}$, and $U^{4+}$.[15] We subsequently developed Zr(IV) chelators obtained either by attaching four optically active amino-functionalized PIPOH derivatives to a calix[4]arene platform[16] or by coupling a carboxylic acid-functionalized PIPOH derivative to the primary amine terminal residue of desferriferrioxamine B.[17]

We now wish to disclose the results of the structural coordination chemistry studies that we carried out with the trivalent metal cations $Fe^{3+}$, and $Ga^{3+}$, a diamagnetic analog of $Fe^{3+}$, with the cyclic hydroxamic acids PIPOH and AZEPOH. Below, we propose to provide a detailed comparison of the structures of the iron and gallium complexes, and an NMR characterization in solution of the gallium complexes. As pointed out in the literature, the interest of studying the coordination chemistry of $Ga^{3+}$ by siderophore analogs also stems from the fact that this trivalent cation could play the role of an antimicrobial agent, by competing with $Fe^{3+}$ in siderophore metal uptake.[18] A patent application concerning gallium complexes that can be given orally to achieve high levels of Ga(III) for the treatment of hypercalcemia of malignancy and related disorders of metabolism can be found in the literature.[19] Interestingly, $[Ga(PIPO)_3]$ and $[Ga(AZEPO)_3]$ were covered by this invention.

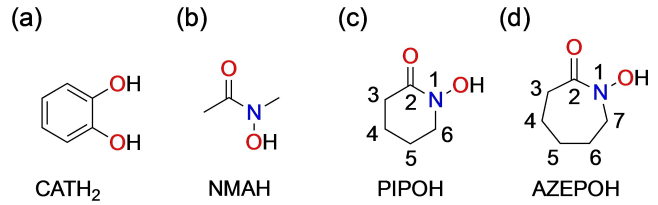


**Figure 2.** Non-functionalized models (protonated forms) of ligand subunits found in siderophores. Atom numbering is shown for the cyclic hydroxamic acids of this study (c and d).

## Results and Discussion

**1. Ligand synthesis and characterization**. PIPOH could be obtained in 70% yield by direct oxidation of piperidine with dimethyldioxirane[13c] and AZEPOH by oxidation of trimethylsilylated ε-caprolactam with $MoO_5$·HMPA (23% yield) followed by EDTA decomplexation.[14a,b] PIPOH could be also obtained in ca. 20% yield by reaction of cyclopentanone with $PhSO_2NH(OH)$ (Piloty's acid) in basic conditions,[13a] a procedure that has been patented.[13b] As this ring expansion reaction does not work when cyclohexanone is employed as starting material,[13d] we followed the method of Spino and Lessard, who reported the synthesis of PIPOBn and AZEPOBn in three steps, starting from δ-valerolactone (**1**) and ε-caprolactone (**2**), respectively (Scheme 1).[14c] The first step involved opening of the lactones by nucleophilic attack of benzylhydroxylamine in the presence of $AlMe_3$. The resulting alcohols (resp. **3** and **4**) were then

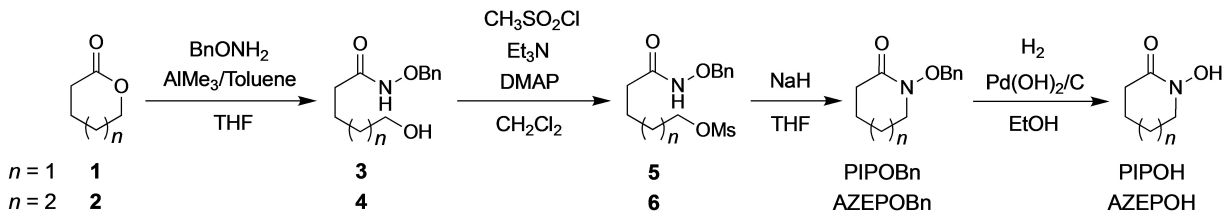


**Scheme 1.** Synthetic routes to PIPOH and AZEPOH from δ-valerolactone (**1**) and ε-caprolactone (**2**), respectively.[14c]

Research Article
doi.org/10.1002/ejic.202300038


converted into the corresponding mesylates (resp. **5** and **6**) using standard conditions. Finally, intramolecular cyclization of the corresponding deprotonated (NaH) benzyloxyamides produced the benzyl-protected heterocycles PIPOBn and AZEPOBn. Whereas all three steps showed fairly good yields in the case of PIPOBn (38% overall yield), this was no longer true for AZEPOBn (23% overall yield). The benzyl-protected hydroxamic acids were purified by column chromatography. PIPOH and AZEPOH were obtained quantitatively by hydrogenolysis in mild conditions (1 atm $H_2$, 20% $Pd(OH)_2/C$) and used without further purification for the complexation reactions. In particular, the purity of PIPOH obtained in this way was the same as the purity of PIPOH obtained by the Piloty's acid method, as shown by comparison of their $^1H$ NMR spectra (Figures S1–S2). The $^1H$ and $^{13}C$ spectra of AZEPOH were fully assigned by using HSQC and HMBC $^{13}C/^1H$ correlations (Figures S3–S10). Interestingly, the $^1H$ NMR spectrum of AZEPOH in acetone-$d_6$ is better resolved than in $CDCl_3$, in which the signal of 7-H show broad features and those of 5-H and 6-H overlap. Examination of the $^1H$ NMR spectra of the intermediates **3**–**6** (Figures S13–S19 and S21–S25) showed that each of the four compounds exists as a mixture of *cis* and *trans* conformers, which give separate signals at 300 K and one set of signals at 330 K in $CDCl_3$. This is interesting to note in keeping with the known *cis*/*trans* isomerism of hydroxamic acids.[20] The NMR spectra of PIPOBn and AZEPOBn are reproduced in Figures S27–S31.

The IR spectra of PIPOH and AZEPOH show a very strong and broad absorption of the carbonyl function at 1604 and 1614 $cm^{-1}$, respectively. The absorption energy of the N–O bond[21] is higher in the case of PIPOH (1093 $cm^{-1}$) than in the case of the seven-membered ring system (1045 $cm^{-1}$). Comparison of the NMR spectra of PIPOH and AZEPOH shows that insertion of a methylene group results in the shift to higher frequencies of the signals of the observed proton ($CH_2$(CO) and $CH_2$N) and carbon (*C*O, $CH_2$(CO), and $CH_2$N) atoms. The $CH_2$(CO) carbon of AZEPOH shows the highest deshielding (+ 11%).

The X-ray crystal structures of the free ligands PIPOH and AZEPOH have been reported in a previous study.[15] The six-membered ring PIPOH shows a half-chair conformation, with 4-C being the most out-of-plane atom, and the seven-membered ring AZEPOH is in slightly distorted chair conformation along the line passing through 5-C and bissecting the N–C(O) bond.

**2. Preparation and spectroscopic properties of the complexes**. The trivalent metal complexes $[ML_3]$ were prepared by mixing stoichiometric amounts of $[M(acac)_3]$ (M = Fe or Ga) and LH (LH = PIPOH and AZEPOH) in methanol. After completion of the reaction, the solvent was removed in vacuum and the residue was crystallized by slow evaporation of a solution of the complex in dichloromethane/heptane or dichloromethane/cyclohexane. Complexes with seven-membered ring ligands were obtained in higher than 90% isolated yields, whereas $[Fe(PIPO)_3]$ and $[Ga(PIPO)_3]$ were isolated in 41% and 54% yields, respectively, after recrystallization.

The complexes were examined and characterized by ESI mass spectrometry, FT-MIR, $^1H$ and $^{13}C$ NMR spectroscopy, and for $[Fe(PIPO)_3]$ by X-band EPR spectroscopy (Figures S33–S50). ESI-MS, NMR, and IR data are collected in Table S1. The main signals in the ESI-MS in the positive mode correspond to the sodium adducts $[ML_3 + Na]^+$ and $[2(ML_3) + Na]^+$. Also observed is the signal of the cationic dihydroxamate species $[ML_2]^+$ resulting from the loss of one ligand, and which has a significant intensity in the case of $[Fe(PIPO)_3]$, as also observed for $[Fe(NMA)_3]$.[12d]

As previously noted for tetravalent metal complexes of $PIPO^-$, complexation shifts $\tilde{\nu}_{CO}$ to lower energy because the carbonyl bond has lost part of its double bond character upon metal coordination. Whereas this shift is negligible in the case of $[Ga(PIPO)_3]$ (+3 $cm^{-1}$), it increases in the order $[Fe(PIPO)_3] < [Ga(AZEPO)_3] < [Fe(AZEPO)_3]$ from −15 to −34 $cm^{-1}$. For a given ligand, the larger bathochromic shift observed in the case of the $Fe^{3+}$ complex by comparison with the $Ga^{3+}$ complex could be explained by a higher covalent character of the iron-oxygen bond, due to $p_\pi$–$d_\pi$ bonding. From the viewpoint of the ligand, the $\tilde{\nu}_{CO}$ shift increases in the order PIPOH < AZEPOH. We note that a shift of −14 $cm^{-1}$, close to the value observed in the case of Fe, had been measured after adsorption of $PIPO^-$ on $TiO_2$.[21]

The EPR spectrum of $[Fe(PIPO)_3]$ in frozen solution (water/ethylene glycol 4:1 v/v, $T$ = 100 K) shown in Figure S35 is characteristic for a nearly rhombic environment in accordance with $g$ factors of 4.29 and 9.27. Hence, it can be safely concluded that the $d^5$ iron center has a high-spin configuration ($S$ = 5/2), as typically found for other ferric siderochelate complexes, including the closely related $[Fe(NMA)_3]$.[12d]

The gallium complexes were characterized in solution by NMR spectroscopy in $CDCl_3$. Selected data are collected in Table S1. Considering that $Ga^{3+}$ has a pseudo-octahedral coordination sphere (see below), two coordination isomers are expected for unsymmetrical ligands like hydroxamates, namely a facial (*fac*) and a meridional (*mer*) one. The *fac* isomer has $C_3$ symmetry, making all three chelates equivalent, whereas they are, in principle, all different in the *mer* isomer ($C_1$ symmetry), giving rise to three sets of signals per inequivalent protons. In addition, each geometrical isomer of a trischelate complex exists in two enantiomeric forms, having either a Λ (left-handed orientation of the three chelate rings) or a Δ (right-handed orientation) configuration. For labile $d^{10}$ metal cations like $Ga^{3+}$, interconversion of both enantiomers without disconnecting a metal-ligand bond is expected to be a fast process achieved through either a trigonal (Bailar)[22] or a rhombic (Rây-Dutt)[23] twist, both passing through a trigonal prismatic transition state. The Bailar twist corresponds to a rotation around the $C_3$ or $C_1$ axis of the *fac* and *mer* isomers, respectively, and thus interconverts both sets of enantiomers only (Λ-*fac* ⇆ Δ-*fac* and Λ-*mer* ⇆ Δ-*mer*). It follows that the three sets of resonances expected in the slow exchange regime for each inequivalent proton of the *mer* isomer reduces to only two sets of signals integrating 1:2 once the rate of inversion of configuration becomes faster than the NMR observation frequency.[24] According to the alternative Rây-Dutt twist mechanism, axial and equatorial donor atoms belonging to the same chelate ring mutually exchange their positions. As this concerted interchange occurs simultaneously within the two chelate rings involving axial donors, the transition state structure assumes also trigonal prismatic geometry. However, it can be easily

Research Article
doi.org/10.1002/ejic.202300038


shown that the Λ-*mer* stereoisomer interconverts into the Δ-*mer* enantiomer and vice versa, giving rise to an inversion of configuration, while the Λ-*fac* complex interconverts into the Δ-*mer* isomer and Δ-*fac* into Λ-*mer*, respectively.

Within the hard-sphere model approximation, Rodger and Johnson have shown that the Bailar twist is energetically favored for rigid ligands having small O–M–O bite angles, as these stabilize trigonal prismatic geometry, while the Rây-Dutt mechanism is favored in the reverse situation.[25] The ratio of the interatomic distance between the pair of donors belonging to the same chelate ring (bite size *b*) over the distance between the nearest-neighbor ligating atoms belonging to different chelates (*l*) can be used as a geometric criterion for predicting the most favorable twist mechanism. Complexes with small *b*/*l* values (typically $b/l < 0.5$) most likely undergo a Bailar twist, while interconversion is expected to proceed via a Rây-Dutt twist for *b*/*l* values close or higher than 1.5. For intermediate values of $b/l \sim 1$, both mechanisms can operate because of similar activation energies. The analysis of the coordination polyhedra of [Ga(PIPO)$_3$] (average $b/l = 0.92$) and [Ga(AZEPO)$_3$] (average $b/l = 0.91$) found in the crystal state (see below) clearly suggest that the Bailar and Rây-Dutt transition states should have similar energies for both complexes, allowing them to invert their configuration but also isomerize at similar rates. Under such circumstances and provided that both nondissociative twist motions are fast on the NMR time scale, all four possible stereoisomers exchange rapidly and a single signal is observed for each inequivalent nucleus, as all three chelating ligands are equivalent.

In order to investigate the possibility of slow exchange between the *fac* and the *mer* stereoisomers of the gallium complexes, we followed the evolution of the $^1$H NMR spectra of [Ga(AZEPO)$_3$] in $CD_2Cl_2$ between 298 and 193 K. A stacked plot of the recorded spectra is shown in Figure S50. As the temperature was decreased down to 193 K, we only observed broadening and loss of resolution of all the signals together with a slight high-field shift, suggesting that all stereoisomers are in fast exchange at temperatures above 190 K in $CD_2Cl_2$. The behavior of [Ga(AZEPO)$_3$] differs from that of [Ga(α-$C_3H_5T$)$_3$] (α-$C_3H_5T$ is α-isopropenyltropolonate), which showed the splitting of the broad singlet of the methyl protons at 285 K into two sets of signals at 190 K, one corresponding to the *fac* stereoisomer and three (including two degenerate) corresponding to the *mer* stereoisomer.[26]

The complexation induced shifts (CIS) of [Ga(PIPO)$_3$] and [Ga(AZEPO)$_3$] have been calculated from Tables S2 and S3 and are compared in Figure 3. Larger and significant shifts are observed by $^{13}$C NMR. Interestingly, they decrease as the topological distance of the carbon atoms to the bound oxygen atoms increases. In addition, the shift is positive for the carbon atoms α to the nitrogen atoms (respectively 6- and 7-C), and negative for the carbonyl C, and the carbon atom α to the carbonyl group (3-C). The CIS observed in the $^1$H NMR spectra are always positive for the corresponding protons ($CH_2CO$ and $CH_2N$).

**3. Structural characterization of the complexes in the solid state: X-ray crystallography studies**. Single crystals of [Fe-

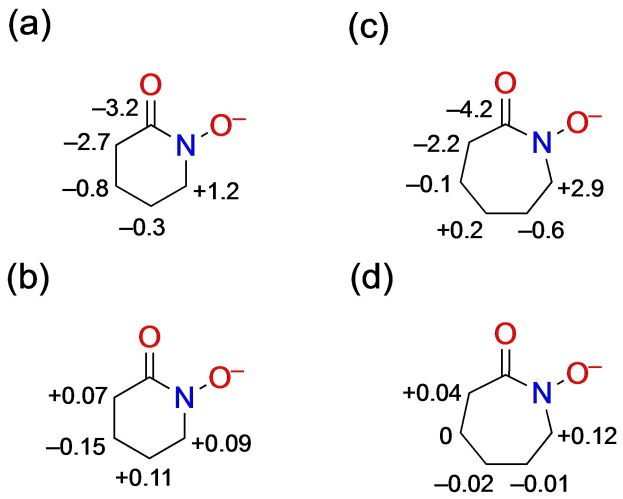


**Figure 3.** CIS measured by comparison of the NMR spectra: (a) $^{13}$C and (b) $^1$H of [Ga(PIPO)$_3$] vs. PIPOH; (c) $^{13}$C and (d) $^1$H of [Ga(AZEPO)$_3$] vs. AZEPOH.

(PIPO)$_3$]·3$CH_2Cl_2$, [Ga(PIPO)$_3$]·benzene sulfonamide, [Fe(AZEPO)$_3$], and [Ga(AZEPO)$_3$], were examined by X-ray diffraction analysis (Table S4). Interestingly, [Fe(PIPO)$_3$]·3$CH_2Cl_2$ reproducibly crystallized in the chiral *P* 321 space group, with $Z = 1$ and a refined Flack parameter of −0.01(1). As the unit cell of the diffracted single crystal contains only the Δ stereoisomer, a most unexpected spontaneous resolution of the racemic mixture occurred upon crystallization. Indeed, the helical arrangement of the three achiral PIPO$^-$ chelates around the iron center in a pseudo-octahedral geometry (see below) affords a racemic mixture of both Λ and Δ enantiomers. With a high-spin $d^5$ electronic configuration, iron(III) complexes are not stabilized by the ligand field and therefore fast Λ ⇆ Δ inversion for [Fe(PIPO)$_3$] is expected too. Hence, albeit fascinating, the exact reasons for the spontaneous resolution remain unclear at that stage. A tentative explanation might be found by analyzing the packing diagram. It shows a layered arrangement of complex molecules in the (*a*,*b*) planes, with co-crystallized dichloromethane molecules sandwiched in-between, giving rise to a network of short CH···Cl (2.85 Å) and ClCH···O (2.44 and 2.56 Å) interactions, which could favor the growth of chiral crystals.

The ORTEP views corresponding to the four structures are gathered together in Figure 4 (Fe complexes) and Figure 5 (Ga complexes). It is important to note that in each complex the nitrogen and carbon atoms of the hydroxamate binding motifs are almost every time disordered over two positions, with site occupation factors set to 0.5, supporting the co-crystallization of the statistical mixture (25/75 %) of both *fac* and *mer* isomers, respectively. Moreover, in the case of the [Ga(PIPO)$_3$] complex, one hydroxamate chelate exhibits two slightly disordered methylenic carbon atoms, which are spread over two positions with occupancies of 0.73 (C3 and C4) and 0.27 (C3* and C4*). Only the major form is displayed in Figure 5.

The conformations of the PIPO$^-$ and AZEPO$^-$ cycles in the complexes were assessed by comparison of the endocyclic torsion angles with those of cyclohexane and cycloheptane,

Research Article
doi.org/10.1002/ejic.202300038



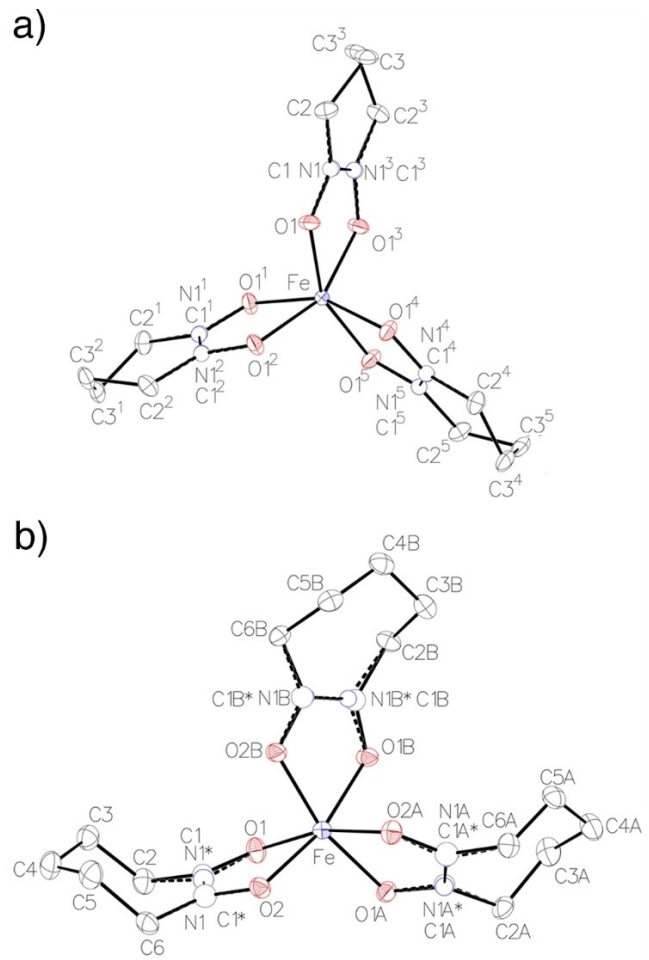


**Figure 4.** ORTEP views of (a) [Fe(PIPO)$_3$] and (b) [Fe(AZEPO)$_3$]. Thermal ellipsoids are drawn at the 50% probability level. H-atoms and solvent molecules are omitted for clarity. The disordered C/N atoms have site-occupation factors (sof) of 0.5; dotted bonds correspond to the second isomer. Symmetry transformations used to generate equivalent atoms of [Fe(PIPO)$_3$]: (1) *y*, *x*, −*z*; (2) −*x*, −*x*+*y*, −*z*; (3) *x*−*y*, −*y*, −*z*; (4) −*y*, *x*–*y*, *z*; (5) −*x*+*y*, −*x*, *z*; (6) *y*, *x*, 1–*z*. For [Fe(AZEPO)$_3$], the starred labels correspond to the disordered positions.

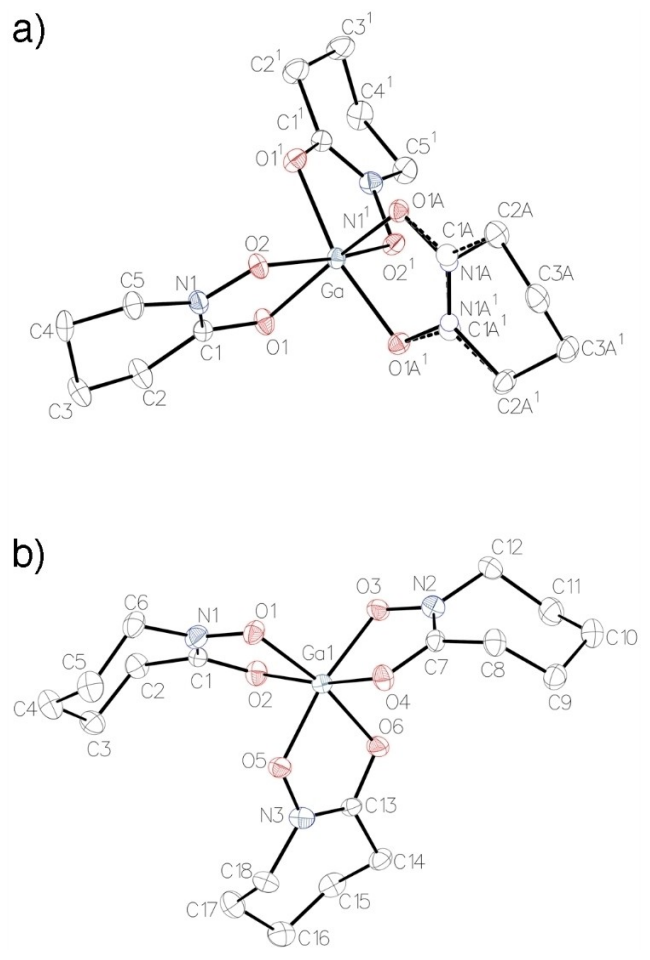


**Figure 5.** ORTEP views of (a) the major form of [Ga(PIPO)$_3$] and (b) [Ga(AZEPO)$_3$]. Thermal ellipsoids are drawn at the 50% probability level. H-atoms and the co-crystallized benzene sulphonamide molecule in (a) are omitted for clarity. Symmetry transformations used to generate equivalent atoms of [Ga(PIPO)$_3$]: (1) 1–*x*, *y*, $^1/_2$–*z*. The disordered C/N atoms have site-occupation factors (sof) of 0.5; dotted bonds correspond to the second isomer.

respectively, and by ring-puckering analysis (Tables S4–S7). For [Ga(PIPO)$_3$] and [Fe(PIPO)$_3$], the six-membered rings adopt half-chair conformations as found in the free ligand,[15] while the AZEPO$^-$ moieties in both gallium and iron complexes take up a chair conformation.

Table 1 gives the bond distances in the five-membered chelate rings of the complexes, together with those corresponding to the free ligands. For both PIPO$^-$ and AZEPO$^-$ ligands, the average metal-oxygen distances are shorter by 0.038 Å in the case of the gallium as compared to the iron complexes. The ionic radius of six-coordinate high-spin $Fe^{3+}$ (0.645 Å) being slightly greater than that of $Ga^{3+}$ (0.62 Å), Fe–O bonds are

**Table 1.** Selected bond distances in the [ML$_3$] complexes and in the free ligands.

| Compound | M–O$_C$/Å[a] | M–O$_N$/Å[a] | M–O/Å[a] | C=O/Å | N–O/Å | C–N/Å |
|---|---|---|---|---|---|---|
| PIPOH[b] | – | – | – | 1.247(2) | 1.397(1) | 1.332(2) |
| [Fe(PIPO)$_3$] | 2.025(2) | 2.025(2) | 2.025(2) | 1.282(11) | 1.379(9) | 1.315(6) |
| [Ga(PIPO)$_3$] | 2.012(2) | 1.962(1) | 1.987(35) | 1.299(12) | 1.368(13) | 1.306(3) |
| AZEPOH[b] | – | – | – | 1.243(3) | 1.399(2) | 1.335(3) |
| [Fe(AZEPO)$_3$] | 2.014(10) | 2.014(10) | 2.014(10) | 1.290(3) | 1.359(4) | 1.326(1) |
| [Ga(AZEPO)$_3$] | 1.979(12) | 1.972(9) | 1.976(10) | 1.326(4) | 1.337(4) | 1.303(1) |

[a] Average values. [b] See Ref. [15].

Research Article
doi.org/10.1002/ejic.202300038


expected to be longer than the Ga–O ones, as observed for the considered hydroxamato complexes. It follows that electrostatic interactions should be weaker in the iron complexes. The Ga–$O_C$ distances are slightly elongated by comparison with the Ga–$O_N$ distances. Upon metal coordination, the C=O bond distances increase whereas the N–O and C–N bond distances decrease. The distance variations depend both on the nature of the ligand and the metal. With two exceptions, the variations are always larger in the case of AZEPOH by comparison with PIPOH, and gallium by comparison with iron. For example in the case of [M(AZEPO)$_3$], $\Delta d$(CO) = 0.047 Å for M = Fe and 0.083 Å for M = Ga, whereas $\Delta d$(NO) = −0.040 Å (Fe) and −0.062 Å (Ga), and $\Delta d$(CN) = −0.009 Å (Fe) and −0.032 Å (Ga). These complexation-induced variations of bond distances within the five-membered chelate ring can be explained by the mesomer effect (Figure 6). In the mesomer form B, the electron density has moved from the nitrogen atom to the carbonyl oxygen atom of the mesomer form A. The result is the lengthening of the CO bond, which has a single bond character, a shortening of both the CN bond, which has a double bond character, and the NO bond, because of enhanced electrostatic interactions between the N and O atoms. As a result of these charge shifts, the carbonyl oxygen atoms carry more electron density.

The coordination geometries were analyzed by the application of the continuous symmetry measure (CSM) approach introduced by Pinsky and Avnir.[27–29] In the four complexes studied, the metal cation is bound to six oxygen atoms. The corresponding coordination polyhedra are generally described in terms of four idealized geometries with equal distances between the center and all vertices (i.e. uniform M–O distances): the hexagon (HP), the pentagonal pyramid (PPY), the octahedron (OC), and the trigonal prism (TPR). As a general approach, shape analysis of coordination polyhedra provides a quantitative mean for evaluating the departure of an experimental (*Q*) from an ideal archetypal stereochemistry (*P*). The Continuous Shape Measure (CShM) criterion $S_Q(P)$ introduced by Avnir, Alvarez, and coworkers reflects the minimal normalized square deviation between the Cartesian coordinates of each vertex belonging to the actual coordination polyhedron *Q* and a perfect reference geometry *P*.[30] Accordingly, $S_Q(P)$ ranges between 0 and 100, a closer structural match giving a lower $S_Q(P)$ value.

We used the Shape program version 2.1, which takes into account the four aforementioned six-vertex polyhedra. Table 2 collects the CShM parameters that have been computed for the four complexes, together with the values found for both molecules of [Fe(NMA)$_3$] co-crystallized in the asymmetric unit of [Fe(NMA)$_3$]·$H_2O$.[12d] Accordingly, the coordination polyhedron adopts in each case a distorted octahedral shape.

The CShM parameters $S_Q$(OC) and $S_Q$(TPR), calculated for all complexes of this study have been placed on the shape map for hexacoordinated complexes in the OC/TPR space (Figure 7). Clearly, the geometry of the coordination sphere of [Fe(PIPO)$_3$] is nearly half-way between OC and TPR, with a small preference for OC, while [Ga(AZEPO)$_3$] has a pronounced preference for OC, as [Fe(AZEPO)$_3$] and one of the [Fe(NMA)$_3$] forms, and [Ga(PIPO)$_3$], albeit to a lesser extent. It is important to note that the apparent intermediate situation of [Fe(PIPO)$_3$] could be due in some part to the structural disorder affecting the nitrogen and carbon atoms of the five-membered ring chelate.

Next, we determined and compared the stereochemical parameters of the OC/TPR geometries of the [ML$_3$] complexes. These parameters are defined in Figure 8. Assuming that the complexes are viewed down the pseudo-$C_3$ symmetry axis, two sets of three oxygen atoms belonging to each of the three ligands define a plane each (Ct and Ct′ are the centroids of the corresponding triangular faces). The stereochemical parameters[31,32] describing the coordination geometries of the

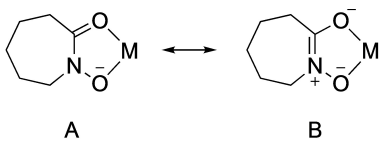


**Figure 6.** Charge shifts within the five-membered ring chelate of $AZEPO^-$.

**Table 2.** Continuous Shape Measure values $S_Q(P)$ calculated for the coordination polyhedra found in the crystal structures of complexes [Fe(NMA)$_3$], [Fe(PIPO)$_3$], [Ga(PIPO)$_3$], [Fe(AZEPO)$_3$], and [Ga(AZEPO)$_3$].

| Complex | $S_Q$(HP) | $S_Q$(PPY) | $S_Q$(OC) | $S_Q$(TPR) |
|---|---|---|---|---|
| [Fe(NMA)$_3$][12d] | 33.89/32.39 | 21.64/22.38 | 2.33/1.58 | 8.15/10.37 |
| [Fe(PIPO)$_3$] | 34.98 | 20.35 | 4.30 | 4.80 |
| [Ga(PIPO)$_3$] | 33.08 | 23.13 | 1.48 | 9.42 |
| [Fe(AZEPO)$_3$] | 32.41 | 22.72 | 1.53 | 10.64 |
| [Ga(AZEPO)$_3$] | 32.28 | 24.83 | 0.81 | 12.02 |

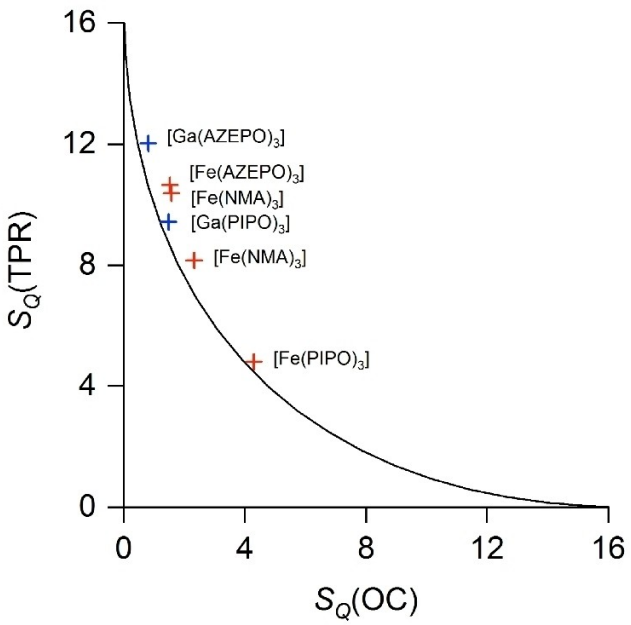


**Figure 7.** Shape map for hexacoordinated complexes showing the minimal distortion interconversion path (solid line) between an octahedron (OC) and a trigonal prism (TPR). Experimental Continuous Shape Measure values $S_Q$(OC) and $S_Q$(TPR) for the iron (red crosses) and gallium (blue crosses) complexes discussed herein are superimposed. For [Fe(NMA)$_3$]·$H_2O$, the asymmetric unit contains two distinct molecules.[12d]

Research Article
doi.org/10.1002/ejic.202300038

Chemistry Europe
European Chemical Societies Publishing

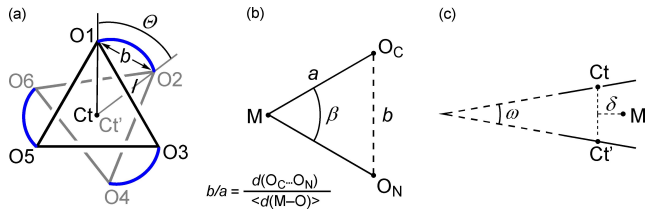


**Figure 8.** Graphical definitions of the stereochemical parameters for the octahedral/trigonal prismatic geometries of $[ML_3]$ complexes, where L is a bidentate chelate (shown as an arc of a circle in blue). M is the metal cation, Ct and Ct′ are the centroids of oxygen donors located in the same plane when the complex is viewed along its pseudo-$C_3$ symmetry axis. (a) Trigonal twist angle $\Theta$ ($\Theta = 60°$ for an ideal OC or 0° for an ideal TPR); (b) bite angle $\beta$ and normalized bite $b/a$; (c) tilt angle $\omega$ between both trigonal faces (O1,O3,O5) and (O2,O4,O6), and lateral metal displacement $\delta$ from the Ct···Ct′ axis.

complexes are: the trigonal twist angle $\Theta$ corresponding to the $O_C$–Ct–Ct′–$O_N$ torsion angle, the average $O_C$–M–$O_N$ bite angle $\beta$, the average normalized bite $b/a$ given by the ratio of the $O_C$···$O_N$ distance ($b$) over the average of the corresponding M–O distances ($a$) for a given chelate ring, the tilt angle $\omega$ between both triangular faces (O1,O3,O5) and (O2,O4,O6), and the lateral metal displacement $\delta$ from the line defined by Ct and Ct′ ($\delta = d(\text{M···Ct}) \times \sin(\angle\text{M···Ct···Ct'})$). These parameters are collected in Table 3. Pictorial representations of the coordination polyhedra of the iron and gallium complexes are shown in Figures 9 and 10, respectively.

Comparison of the values of the stereochemical parameters of Table 3 shows that the bite angle $\beta$ and the normalized bite $b/a$ of the iron complexes are ca. 10% smaller than those of the gallium complexes: on average 79.0° vs. 81.7° for $\beta$ and 1.272 vs. 1.308 for $b/a$, respectively. These values are closer, for the Ga complexes, to those calculated for the perfect octahedron ($\beta = 90°$, $b/a = 1.414$, $\Theta = 60°$, $\omega = 0°$, and $\delta = 0$ Å). The twist angle $\Theta$ of 48.3° measured for $[Ga(AZEPO)_3]$ is the closest to the theoretical value of 60°, while $[Fe(PIPO)_3]$ has the smallest value (30.6°). By contrast, the angle $\omega$ of the planes containing the oxygen centroids has the highest deviation (4.7°) from zero in the case of $[Fe(AZEPO)_3]$, the perfect parallelism of these planes being observed for $[Fe(PIPO)_3]$. In this latter complex, the $Fe^{3+}$ cation is located on the line defined by Ct and Ct′, whereas in the former complex it is off this line by 0.035 Å.

Kepert has devised a very simple method of determination of the stereochemistry of metal complexes, particularly those carrying three bidentate ligands.[32] This approach rests on the minimization of the repulsion interactions between the donor

**Table 3.** Parameters describing the coordination polyhedra of the complexes.

| Complex | $\beta$/° | $b/a$ | Ct···Ct′/Å | $\Theta$/° | $\omega$/° | $\delta$/Å |
|---|---|---|---|---|---|---|
| $[Fe(NMA)_3]$[12d] | 78.7(6) | 1.267 | 2.292 | 39 | 2.7 | 0.020 |
| | 78.7(6) | 1.272 | 2.236 | 44 | 3.3 | 0.031 |
| $[Fe(PIPO)_3]$ | 78.5(4) | 1.266 | 2.415 | 30.6 | 0.0 | 0.000 |
| $[Ga(PIPO)_3]$ | 81.3(2) | 1.303 | 2.287 | 43.2 | 2.2 | 0.036 |
| $[Fe(AZEPO)_3]$ | 79.4(1) | 1.278 | 2.240 | 44.3 | 4.7 | 0.035 |
| $[Ga(AZEPO)_3]$ | 82.0(1) | 1.312 | 2.216 | 48.3 | 3.0 | 0.019 |

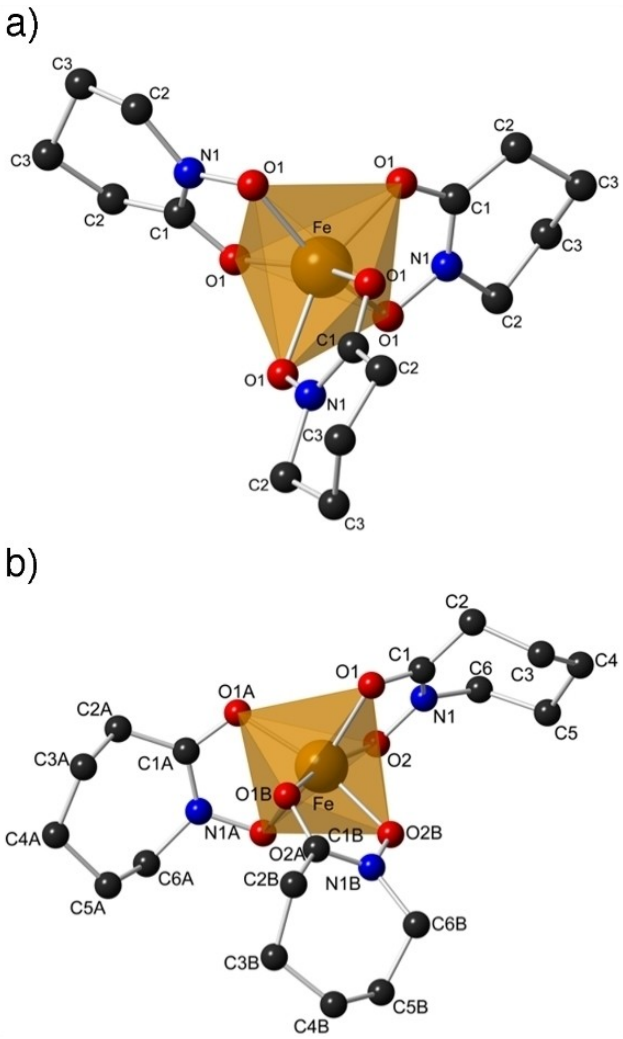


**Figure 9.** Pictorial representations of the coordination polyhedra of (a) $[Fe(PIPO)_3]$ and (b) $[Fe(AZEPO)_3]$.

atoms, considered as points placed on the surface of a sphere of radius $r$, centered on the metal cation. In this simple model, the interaction between any two donor atoms $i$ and $j$ is considered as being exclusively repulsive and proportional to $d_{ij}^{-n}$, where $d_{ij}$ is the distance between them and $n$ is an integer. Usual custom values considered for $n$ are 1 (coulomb potential), 6, and 12. The total interaction energy can be expressed as $U = \Sigma A_n d_{ij}^{-n}$, where $A_n$ is a proportionality constant. Plotting $U = f(\Theta)$ for different values of the normalized bite ($b/a$) produces a set of curves which show a minimum at $\Theta_{min}$. Figure 11 shows the evolution of $\Theta_{min}$, corresponding to the minimization of the ligand repulsion energies for three values of $n$ as a function of the normalized bite $b/a$. The points corresponding to the pairs ($b/a$,$\Theta$) obtained from the X-ray crystal structures of the four complexes solved in this work and that of $[Fe(NMA)_3]$[12d] are superimposed on the curves.

Examination of Figure 11 shows that the points corresponding to $[Fe(PIPO)_3]$, one of the $[Fe(NMA)_3]$ molecules and, to a lesser extent, $[Ga(PIPO)_3]$ are clearly outside the reference

Research Article
doi.org/10.1002/ejic.202300038



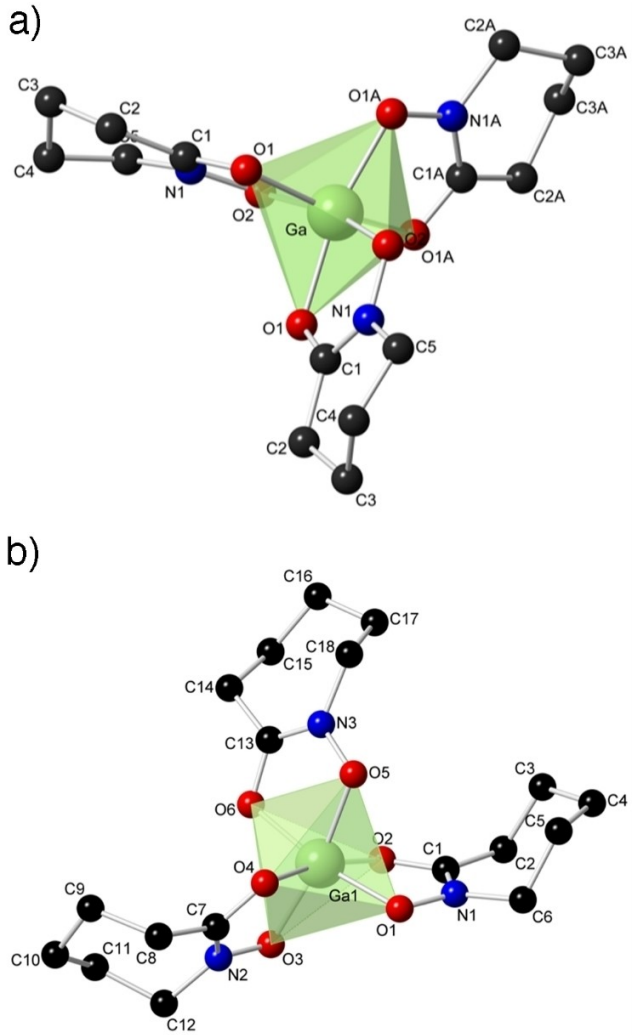


**Figure 10.** Pictorial representations of the coordination polyhedra of (a) $[Ga(PIPO)_3]$ and (b) $[Ga(AZEPO)_3]$.

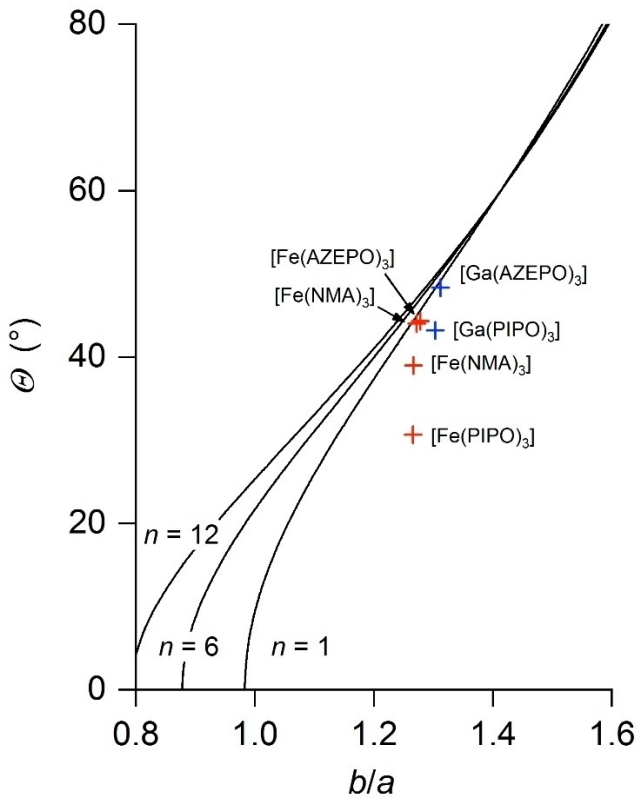


**Figure 11.** Variation of the minimal twist angle $\Theta_{min}$ calculated according to the repulsion model proposed by Kepert as a function of the normalized bite *b*/*a* for three different values of *n*. Experimental values for the iron (red crosses) and gallium (blue crosses) complexes discussed herein are superimposed. For $[Fe(NMA)_3]\cdot H_2O$, the asymmetric unit contains two distinct molecules.[12d]

curves, the deviation being larger for structures coming closer to the TPR coordination geometry. In contrast, the twist angle found for the complex with the seven-membered ring hydroxamate $AZEPO^-$ is very close to the reference curve corresponding to $n = 1$. These simple structural considerations indicate that $AZEPO^-$ generates $[ML_3]$ complexes with trivalent metals that are less strained than their $PIPO^-$ homologs.

Interestingly, the X-ray crystal structure of the $Fe^{3+}$ complex of amychelin, a siderophore of tripodal topology containing three different chelates, one derived from 2-(4,5-dihydro-2-oxazolyl)-phenol, one from acetohydroxamic acid (AHA), and one from PIPOH was determined at 0.84 Å resolution.[33] As found herein, the cyclic D-*N*-$O^-$-Orn moiety that derives from $PIPO^-$ assumes also a half-chair conformation in the iron complex. The metal cation has a distorted octahedral coordination geometry, in which the $(N)O^-$ oxygen donors are arranged *trans* to each other. The bond distances in the hydroxamate chelates deriving from the $PIPO^-$ and acetohydroxamate fragments are 2.002 and 1.979 Å for Fe–$O_N$, 2.077 and 2.070 Å for Fe–$O_C$, respectively. Interestingly, the Fe–$O_C$ bonds could be distinguished from the Fe–$O_N$ ones, as the former was significantly longer than the latter. However, the average Fe–O bond distance for the Fe/$PIPO^-$ chelate ring of ferriamychelin (2.040 Å) was longer than the average Fe–O bond lengths in $[Fe(PIPO)_3]$ (2.025 Å).

## Conclusion

In this study, we have examined the spectroscopic and structural characteristics of the complexes of two cyclic hydroxamate ligands, the six-membered ring $PIPO^-$, and the seven-membered ring $AZEPO^-$ with selected trivalent metals, $Fe^{3+}$ and $Ga^{3+}$, the latter being a diamagnetic surrogate of $Fe^{3+}$. The significance of these ligands arises from the fact that they represent models of terminal hydroxamate subunits in many natural siderophores, including the rich families of mycobactins and exochelins.

In chloroform solutions and down to ca. 200 K, both labile trischelate $d^{10}$ complexes $[Ga(PIPO)_3]$ and $[Ga(AZEPO)_3]$ undergo, at the NMR frequency scale, fast $\Lambda/\Delta$ interconversion and *fac*/*mer* isomerization without bond breaking according to the

trigonal Bailar and rhombic Rây-Dutt twist mechanisms. Relying on the structural analysis of their coordination polyhedra, both interchange processes are predicted to occur simultaneously with similar activation energies. Likewise, the lack of ligand-field stabilization energy confers a high lability to the corresponding high-spin $d^5$ ferric counterparts, which are thus expected to rearrange rapidly too.

The structures of the four complexes synthesized could be determined by single crystal X-ray diffraction analysis. The data showed that the coordination geometries of the $AZEPO^-$ complexes are closer to an octahedron than those of the $PIPO^-$ complexes, the geometry of $[Fe(PIPO)_3]$ being half-way between the octahedron and the trigonal prism. In addition, the Fe–O distances of $[Fe(AZEPO)_3]$ were 0.01 Å shorter by comparison with those of $[Fe(PIPO)_3]$, suggesting that the Fe–O coordination bonds are stronger in the former than in the latter. Comparative studies on the solution thermodynamics and kinetics of $[Fe(PIPO)_3]$ and $[Fe(AZEPO)_3]$ are in progress and will be disclosed in due course.

## Experimental Section

**Methods and Instrumentation**: Physical measurements were performed either at the technological platform for chemical analysis and molecular synthesis of the Institut de Chimie Moléculaire de l'Université de Bourgogne (PACSMUB, http://www.wpcm.fr) or at the Fédération de Chimie "Le Bel" of the University of Strasbourg. $^1H$ and $^{13}C\{^1H\}$ NMR spectra were recorded on Bruker spectrometers operating either at 500.03 MHz (Bruker Avance III) or 600.23 MHz (Bruker Avance II). Chemical shifts on the $\delta$ scale (ppm) relative to tetramethylsilane were referenced internally with respect to the proton and carbon resonances of either residual $CHCl_3$ ($\delta_H$ = 7.26 ppm and $\delta_C$ = 77.16 ppm) or acetone ($\delta_H$ = 2.05 ppm and $\delta_C$ = 30.60 ppm). Fourier-transform mid-infrared (400–4000 $cm^{-1}$) spectra (FT-MIR) were recorded at 4 $cm^{-1}$ resolution on a Bruker VERTEX 70v spectrometer fitted with an A225 diamond ATR accessory (Bruker) and a DTGS detector (350–4000 $cm^{-1}$).

**Mass spectrometry**: High-resolution electrospray ionization mass spectra (HR-ESI-MS) were recorded on an LTQ XL Orbitrap (Thermo Scientific) machine equipped with an electrospray ionization source (ESI) and the data processed with the Thermo Xcalibur 3.0.63 software.

**Materials**: Unless otherwise stated, the reactions were carried out under an argon atmosphere using Schlenk techniques. The following solvents and reagents were dried and distilled under argon prior to use: acetonitrile (calcium hydride), THF (sodium/benzophenone), dichloromethane (phosphorus pentoxide), and triethylamine (sodium; storage on potassium hydroxide pellets). All other solvents and analytical-grade chemicals were obtained from commercial suppliers and used without further purification. Separations were performed by flash column chromatography using 40–60 μm silicagel 60. 1-(Benzyloxy)piperidine-2-one (PIPOBn) and *N*-benzyloxycaprolactam (AZEPOBn) were prepared according to the literature.[14c] We complete the existing characterization data sets by providing here the full assignment of the $^1H$ and $^{13}C$ NMR spectra, and other data.

***N*-Benzyloxy-5-hydroxypentanamide (3)**: $^1H$ NMR (600 MHz, $CDCl_3$, 300 K): $\delta$ = 8.406 (br s, 1 H; NH), 7.908 (br s, 1 H; NH′), 7.379 (br s, 10 H; o, o′, m, m′, p, p′-H), 4.905 (br s, 2 H; PhC$H_2$), 4.827 (br s, 2 H; PhC$H_2$′), 3.609 (t, $^3J_{H,H}$ = 6.0 Hz, 4 H; 6, 6′-H), 2.393 (br s, 1 H; OH′), 2.099 (br s, 1 H; OH), 1.910 (br s, 2 H; 3′-H), 1.715 (br m, 6 H; 3, 5, 5′-H), 1.558 (apparent quint, $^3J_{H,H}$ = 6.60 Hz; 4, 4′-H) ppm.

***N*-Benzyloxy-5-mesyloxypentanamide (5)**: $^1H$ NMR (600 MHz, $CDCl_3$, 300 K): $\delta$ = 7.383 (br s, 10 H; o, o′, m, m′, p, p′-H), 4.907 (br s, 2 H; PhC$H_2$), 4.839 (br s, 2 H; PhC$H_2$′), 4.212 (apparent quint, $^3J_{H,H}$ = 6.0 Hz, $^4J_{H,H}$ = 2.7 Hz, 4 H; 6, 6′-H), 2.992 (s, 6 H; $CH_3$, $CH_3$′), 2.386 (br s, 2 H; 3′-H), 2.097 (br s, 2 H; 3-H), 1.758 (m, 8 H; 4, 4′, 5, 5′-H) ppm.

**PIPOBn**: $^1H$ NMR (600 MHz, $CDCl_3$, 293 K): $\delta$ = 7.434 (m, $^3J_{H,H}$ = 7.8 Hz, $^4J_{H,H}$ = 1.8 Hz, 2 H; o-H), 7.357 (m, $^3J_{H,H}$ = 7.2 Hz, $^4J_{H,H}$ = 1.8 Hz, 3 H; m, p-H), 4.972 (s, 2 H, $PhCH_2$), 3.324 (t, $^3J_{H,H}$ = 6.0 Hz, 2 H; 6-H), 2.449 (t, $^3J_{H,H}$ = 6.6 Hz, 2 H; 3-H), 1.774 (m, $^3J_{H,H}$ = 6.0 Hz, 2 H; 4-H), 1.705 (m, $^3J_{H,H}$ = 6.0 Hz, 2 H; 5-H) ppm.

**PIPOH**: $^1H$ NMR (600 MHz, $CDCl_3$, 300 K): $\delta$ = 9.039 (v br s, 1 H; OH), 3.620 (t, $^3J_{H,H}$ = 6.6 Hz, 2 H; 6-H), 2.440 (t, $^3J_{H,H}$ = 6.6 Hz, 2 H; 3-H), 1.937 (m, $^3J_{H,H}$ = 6.0 Hz, 2 H; 4-H), 1.796 (m, $^3J_{H,H}$ = 6.6 Hz, 2 H; 5-H) ppm.

***N*-Benzyloxy-6-hydroxyhexanamide (4)**: Oil. IR (ATR): $\tilde{\nu}$ = 3186 (m, br), 2936 (m), 2864 (m), 1650 (s), 1498 (m), 1455 (m), 1365 (m), 1211 (w), 1047 (s), 908 (m), 837 (w), 746 (s), 697 (s) $cm^{-1}$; $^1H$ NMR (600 MHz, $CDCl_3$, 300 K): $\delta$ = 9.322 (s, 1 H; NH), 8.328 (br s, 1 H; NH′), 7.350 (s, 2×3 H; m, p, m′, p′-H), 7.328 (m, 2×2 H; o, o′-H), 4.849 (br s, 2 H; PhC$H_2$), 4.780 (br s, 2 H; PhC$H_2$′), 3.527 (s, 2×2 H; 7, 7′-H), 2.739 (br s, 2×1 H; OH, OH′), 2.322 (br s, 2 H; 3′-H), 2.015 (br t, 2 H; 3-H), 1.581 (apparent quint, $^3J_{H,H}$ = 7.2 Hz, 2×2 H; 4, 4′-H), 1.482 (br apparent quint, $^3J_{H,H}$ = 6.0 Hz, 2×2 H; 6, 6′-H), 1.306 (br apparent quint, 2×2 H; 5, 5′-H) ppm; $^{13}C$ NMR (151 MHz, $CDCl_3$, 300 K): $\delta$ = 171.2 (2, 2′-C), 135.6 (i, i′-C), 129.2 (m, m′-C), 128.7 (p, p′-C), 128.6 (o, o′-C), 78.1 ($PhCH_2$, $PhCH_2$′), 62.3 (7, 7′-C), 33.0 (3, 3′-C), 32.1 (6, 6′-C), 25.2 (5, 5′-C), 25.1 (4, 4′-C) ppm; $^1H$ NMR (600 MHz, $CDCl_3$, 330 K): $\delta$ = 7.84 (br s, 1 H; NH), 7.41-7.34 (m, 5 H; Ph–H), 4.90 (br s, 2 H; PhC$H_2$), 3.64 (t, $^3J_{H,H}$ = 6.6 Hz, 2 H; 7-H), 2.16 (br s, 2 H; 3-H), 1.67 (apparent quint, $^3J_{H,H}$ = 7.5 Hz, 2 H; 4-H), 1.57 (apparent quint, $^3J_{H,H}$ = 7.2 Hz; 6-H), 1.40 (m, 2 H; 5-H) ppm.

***N*-Benzyloxy-6-mesyloxyhexanamide (6)**: Solid, m.p. = 59.1 °C; IR (ATR): $\tilde{\nu}$ = 3166 (m), 2995 (m), 2947 (m), 2864 (m), 1642 (s), 1533 (m), 1454 (m), 1332 (d, s), 1238 (w), 1173 (s), 1111 (w), 1046 (m), 1020 (m), 979 (s), 944 (s), 916 (s), 829 (s), 744 (s), 698 (s) $cm^{-1}$; $^1H$ NMR (600 MHz, $CDCl_3$, 300 K): $\delta$ = 7.950 (br s, 1 H; NH), 7.715 (br s, 1 H; NH′), 7.387 (s, 2×5 H; o, m, p, o′, m′, p′-H), 4.915 (br s, 2×2 H; PhC$H_2$, PhC$H_2$′), 4.214 (t, $^3J_{H,H}$ = 6.6 Hz, 2×2 H; 7, 7′-H), 2.996 (s, 2×3 H; $CH_3$, $CH_3$′), 2.370 (br s, 2 H; 3′-H), 2.058 (br s, 2 H; 3-H), 1.753 (apparent quint, $^3J_{H,H}$ = 7.1 Hz, 2×2 H; 6, 6′-H), 1.671 (br t, 2×2 H; 4, 4′-H), 1.428 (apparent quint, $^3J_{H,H}$ = 7.7 Hz, 2×2 H; 5, 5′-H) ppm; $^{13}C$ NMR (151 MHz, $CDCl_3$, 300 K): $\delta$ = 170.6 (2, 2′-C), 135.5 (i, i′-C), 129.4 (m, m′-C), 129.0 (p, p′-C), 128.9 (o, o′-C), 78.4 ($PhCH_2$, $PhCH_2$′), 69.9 (7, 7′-C), 37.6 ($CH_3$, $CH_3$′), 33.0 (3, 3′-C), 29.0 (6, 6′-C), 25.1 (5, 5′-C), 24.7 (4, 4′-C) ppm; $^1H$ NMR (600 MHz, $CDCl_3$, 330 K): $\delta$ = 7.81 (br s, 1 H; N–H), 7.40–7.35 (m, 5 H; Ph–H), 4.89 (br s, 2 H; PhC$H_2$), 4.22 (t, $^3J_{H,H}$ = 6.3 Hz, 2 H; 7-H), 2.98 (s, 3 H, $CH_3$), 2.16 (br s, 2 H; 3-H), 1.76 (apparent quint, $^3J_{H,H}$ = 7.05 Hz, 2 H; 6-H), 1.68 (apparent quint, $^3J_{H,H}$ = 7.5 Hz, 2 H; 4-H), 1.45 (m, 2 H; 5-H) ppm; elemental analysis calcd (%) for $C_{14}H_{21}NO_5S$ (315.39 g/mol): C 53.32, H 6.71, N 4.44, S 10.17; found: C 53.00, H 6.88, N 4.83, S 9.23.

**AZEPOBn**: Solid, m.p. = 60.2 °C; IR (ATR): $\tilde{\nu}$ = 3074 (vw), 3041 (vw), 2934 (m), 2918 (m), 2881 (w), 2854 (w), 1651 (s), 1497 (w), 1452 (m), 1407 (m), 1380 (w), 1353 (w), 1333 (w), 1293 (w), 1260 (w), 1231 (w), 1218 (w), 1196 (w), 1147 (w), 1077 (w), 1039 (m), 1011 (m), 991 (m), 968 (m), 945 (w), 912 (m), 858 (m), 839 (m), 804 (w), 745 (s), 721 (w), 695 (s) $cm^{-1}$; $^1H$ NMR (600 MHz, $CDCl_3$, 300 K): $\delta$ = 7.430 (m, $^3J_{H,H}$ = 6.3 Hz, $^4J_{H,H}$ = 1.5 Hz, 2 H; o-H), 7.353 (m, 3 H; m, p-H), 4.950 (s, 2 H; PhC$H_2$), 3.512 (apparent quint, $^2J_{H,H}$ = 10.8 Hz, 2 H; 7-H), 2.448 (apparent quint, $^2J_{H,H}$ = 10.8 Hz, 2 H; 3-H), 1.650 (m, 4 H; 4-H, 5-H), 1.502 (apparent quint, $^3J_{H,H}$ = 5.4 Hz, 2 H; 6-H) ppm; $^{13}C$ NMR

Research Article
doi.org/10.1002/ejic.202300038





(151 MHz, $CDCl_3$, 300 K): $\delta = 172.7$ (2-C), 135.9 (i-C), 129.7 (o-C), 128.7 (p-C), 128.5 (m-C), 76.5 ($PhCH_2$), 53.8 (7-C), 36.5 (3-C), 29.8 (5-C), 27.2 (6-C), 23.1 (4-C) ppm.

**AZEPOH**: A mixture of AZEPOBn (0.34 g, 1.57 mmol) and 20% $Pd(OH)_2/C$ (0.015 g) in ethanol (50 mL) was stirred under 1 atm dihydrogen at room temperature. The reaction was followed by TLC ($SiO_2$; EtOAc/hexane, 2:1 v/v). After 3 h stirring, the reaction mixture was filtered through glass microfibers. The filtrate was concentrated at the rotary evaporator. Further drying under vacuum afforded pure AZEPOH as a solid (0.20 g, 99% yield). Crystalline AZEPOH could be obtained by sublimation at 35 °C under vacuum; m.p. 80.7 °C (lit.,[13b] 80–81 °C); IR (ATR): $\tilde{\nu} = 3082$ (br, w; OH), 2931 (m), 2848 (m), 2643 (br, m), 1614 (br, s; CO), 1496 (m), 1471 (m), 1441 (s), 1353 (w), 1334 (w), 1287 (w), 1258 (vw), 1230 (w), 1211 (w), 1191 (sh, w), 1147 (w), 1087 (w), 1045 (m), 1012 (m), 978 (vw), 944 (w), 884 (vw), 854 (m), 814 (m), 782 (br, w), 708 (w), 683 (m) $cm^{-1}$; $^1H$ NMR (600 MHz, $CDCl_3$, 300 K): $\delta = 7.214$ (br s, 1 H; OH), 3.735 (br t, 2 H; 7-H), 2.517 (pseudo-t, $^3J_{H,H} = 5.4$ Hz, 2 H; 3-H), 1.738 (m, 4 H; 5, 6-H), 1.650 (br m, 2 H, 4-H) ppm; $^{13}C$ NMR (151 MHz, $CDCl_3$, 300 K): $\delta = 170.3$ (2-C), 51.4 (7-C), 34.4 (3-C), 29.8 (5-C), 26.7 (6-C), 23.0 (4-C) ppm; $^1H$ NMR (600 MHz, acetone-$d_6$, 300 K): $\delta = 8.504$ (br s, 1 H; OH), 3.708 (apparent sxt, $^2J_{H,H} = 10.20$ Hz, 2 H; 7-H), 2.452 (apparent sxt, $^2J_{H,H} = 12.00$ Hz, 2 H; 3-H), 1.738 (m, 2 H; 5-H), 1.685 (m, 2 H; 6-H), 1.609 (m, 2 H; 4-H) ppm; $^{13}C$ NMR (151 MHz, acetone-$d_6$, 300 K): $\delta = 171.6$ (2-C), 52.5 (7-C), 35.7 (3-C), 31.0 (5-C), 28.3 (6-C), 24.6 (4-C) ppm; HR-MS (ESI): *m/z* calcd for $C_6H_{11}NO_2Na$ ($[L + Na]^+$) 152.0682, found 152.0678; elemental analysis calcd (%) for $C_6H_{11}NO_2$ (129.16 g/mol): C 55.80, H 8.58, N 10.84; found: C 55.16, H 8.68, N 11.33.

**[Fe(PIPO)$_3$]**: A solution of [Fe(acac)$_3$] (0.113 g, 0.32 mmol) in MeOH (40 mL) was transferred via cannula to a solution of PIPOH (0.109 g, 0.95 mmol) in MeOH (70 mL). The reaction mixture was stirred under argon at room temperature overnight. The solvent was removed under reduced pressure. Fractional crystallization from $CH_2Cl_2$/heptane (1:3 v/v) afforded [Fe(PIPO)$_3$] as a red crystalline solid (0.052 g, 41% yield); m.p. 214.7–215.2 °C; IR (ATR): $\tilde{\nu} = 2934$ (m), 2860 (m), 1589 (s; CO), 1474 (s), 1448 (m), 1426 (m), 1351 (m), 1327 (m), 1260 (m), 1107 (m, br), 924 (m), 878 (m), 800 (w, br), 721 (m), 659 (w), 599 (w), 549 (m, br) $cm^{-1}$; HR-MS (ESI): *m/z* calcd for $C_{10}H_{16}N_2O_4Fe$ ($[FeL_2]^+$) 284.0460, found 284.0458; $C_{15}H_{25}N_3O_6Fe$ ($[FeL_3 + H]^+$) 399.1087, found 399.1095; $C_{15}H_{24}N_3O_6FeNa$ ($[FeL_3 + Na]^+$) 421.0907, found 421.0911; $C_{30}H_{48}N_6O_{12}Fe_2Na$ ($[Fe_2L_6 + Na]^+$) 819.1922, found 819.1934; elemental analysis calcd (%) for $C_{15}H_{24}N_3O_6Fe{\cdot}C_7H_{16}{\cdot}CH_2Cl_2{\cdot}H_2O$ (601.36 g/mol): C 45.94, H 7.37, N 6.99; found: C 46.17, H 6.16, N 7.06.

**[Ga(PIPO)$_3$]**: The same procedure starting from [Ga(acac)$_3$] (0.137 g, 0.37 mmol) and PIPOH (0.132 g, 1.12 mmol) afforded [Ga(PIPO)$_3$] as colorless crystals (0.086 g, 54% yield); m.p. 255.0–256.4 °C; IR (ATR): $\tilde{\nu} = 3375$ (s, v br; water), 2949 (m, br), 1607 (vs; CO), 1469 (s), 1448 (m), 1426 (m), 1355 (m), 1332 (m), 1317 (w), 1269 (w), 1224 (w), 1183 (w), 1172 (w), 1107 (m), 1070 (w), 927 (m), 877 (w), 722 (m), 660 (w), 604 (m, sh), 580 (m, br), 475 (w) $cm^{-1}$; $^1H$ NMR (500.13 MHz, $CDCl_3$, 300 K): $\delta = 3.712$ (t, $^3J_{H,H} = 5.5$ Hz, 6 H; 6-H), 2.513 (t, $^3J_{H,H} = 6.0$ Hz, 6 H; 3-H), 1.903 (br m, $^3J_{H,H} = 5.0$ Hz, 6 H; 5-H), 1.785 (br m, $^3J_{H,H} = 6.0$ Hz, 6 H; 4-H) ppm; $^{13}C$ NMR (126 MHz, $CDCl_3$, 300 K): $\delta =$ 161.3 (CO), 50.1 (6-C), 28.2 (3-C), 22.9 (5-C), 20.2 (4-C) ppm; HR-MS (ESI): *m/z* calcd for $C_{15}H_{24}N_3O_6GaNa$ ($[GaL_3 + Na]^+$) 434.0813, found 434.080; $C_{30}H_{48}N_6O_{12}Ga_2Na$ ($[Ga_2L_6 + Na]^+$) 847.1729, found 847.1701; elemental analysis calcd (%) for $C_{15}H_{24}N_3O_6Ga{\cdot}CH_2Cl_2$ (497.02 g/mol): C 38.66, H 5.27, N 8.45; found: C 38.48, H 5.83, N 8.51.

**[Fe(AZEPO)$_3$]**: A solution of [Fe(acac)$_3$] (0.126 g, 0.36 mmol) in MeOH (6 mL) was mixed with a solution of AZEPOH (0.128 g, 0.99 mmol) in MeOH (15 mL). The reaction mixture was stirred under air at room temperature and its progress monitored by TLC ($SiO_2$; $CH_2Cl_2$/MeOH, 90:10 v/v). The reaction was complete after 4 h. The solvent was removed by rotary evaporation and the residue dissolved in dichloromethane (10 mL). Heptane (1.2 mL) was added as counter-solvent and the solution allowed to concentrate gently. After two weeks, red crystals had formed. The supernatant solution was removed. The crystals were washed with heptane and dried in vacuum. This procedure afforded pure [Fe(AZEPO)$_3$] (0.148 g, 93% yield). IR (ATR): $\tilde{\nu} = 2829$ (m), 2854 (w), 1580 (vs; CO), 1529 (sh, w), 1471 (s), 1442 (br, m), 1351 (w), 1286 (w), 1240 (w), 1207 (w), 1152 (w), 1117 (w), 1085 (w), 1051 (m), 1018 (m), 992 (sh, w), 948 (w), 887 (vw), 848 (m), 813 (m), 777 (vw), 741 (br, vw) $cm^{-1}$.

**[Ga(AZEPO)$_3$]**: A solution of [Ga(acac)$_3$] (0.051 g, 0.14 mmol) in MeOH (10 mL) was mixed with a solution of AZEPOH (0.054 g, 0.42 mmol) in MeOH (10 mL). After stirring overnight, the solvent was removed by rotary evaporation to afford a crude material that was reprecipitated from $CH_2Cl_2$/cyclohexane. Pure [Ga(AZEPO)$_3$] was isolated as a colorless solid (0.060 g, 94% yield). Single crystals suitable for the single crystal X-ray diffraction analysis were obtained by slow evaporation of a $CH_2Cl_2$/cyclohexane (1:1 v/v) solution of [Ga(AZEPO)$_3$]. IR (ATR): $\tilde{\nu} = 2927$ (m), 1596 (s; CO), 1472 (m), 1205 (w), 1052 (m), 1017 (m), 949 (w), 850 (m), 812 (m), 691 (m), 612 (m), 580 (br, m), 425 (w) $cm^{-1}$; $^1H$ NMR (500 MHz, $CDCl_3$, 298 K): $\delta = 3.857$ (pseudo t, $^3J_{H,H} = 5.0$ Hz, 6 H; 7-H), 2.558 (pseudo t, $^3J_{H,H} = 5.0$ Hz, 6 H; 3-H), 1.727 (br m, 6 H; 6-H), 1.718 (br m, 6 H; 5-H) 1.652 (br apparent quint, $^3J_{H,H} = 4.5$ Hz, 6 H; 4-H) ppm; $^{13}C$ NMR (126 MHz, $CDCl_3$, 295 K): $\delta = 166.1$ (2-C), 54.3 (7-C), 32.2 (3-C), 29.9 (5-C), 26.1 (6-C), 23.9 (4-C) ppm; HR-MS (ESI): *m/z* calcd for $C_{18}H_{30}N_3O_6GaNa$ ($[GaL_3 + Na]^+$) 476.1283, found 476.1286; $C_{36}H_{60}N_6O_{12}Ga_2Na$ ($[Ga_2L_6 + Na]^+$) 931.2669, found 931.2763; elemental analysis calcd (%) for $C_{18}H_{30}N_3O_6Ga{\cdot}0.5H_2O$ (463.18 g/mol): C 46.68, H 6.75, N 9.07; found: C 46.83, H 6.71, N 9.21.

Deposition Numbers 1823831 (for [Fe(PIPO)$_3$]), 1823832 (for [Ga(PIPO)$_3$]), 1823833 (for [Fe(AZEPO)$_3$]), 2056438 (for [Ga(AZEPO)$_3$]) contain the supplementary crystallographic data for this paper. These data are provided free of charge by the joint Cambridge Crystallographic Data Centre and Fachinformationszentrum Karlsruhe Access Structures service.

## Acknowledgements

*This work was financially supported by the Centre National de la Recherche Scientifique (CNRS), the Conseil Régional de Bourgogne (CRB, program PARI II CDEA), the European Regional Development Fund (FEDER), the European Union funded ERASMUS + Traineeship program (A.M.C. T.), the French program "NEEDS Environnement" (project ACTISOL), and the Agence Nationale de la Recherche (ANR project PLUTON, grant N° ANR-17-CE08-0053). We are grateful to Mrs. Marie-Joëlle Eymin for assistance with ligand synthesis and to Dr. Stéphane Brandès for recording EPR spectra.*

## Conflict of Interest

The authors declare no conflict of interest.

Research Article
doi.org/10.1002/ejic.202300038



## Data Availability Statement

The data that support the findings of this study are available in the supplementary material of this article.

**Keywords:** coordination modes · gallium · hydroxamic acid · iron · siderophore

[1] a) L. D. Loomis, K. N. Raymond, *Inorg. Chem.* **1991**, *30*, 906–911; b) K. N. Raymond, G. Müller, B. F. Matzanke, *Top. Curr. Chem.* **1984**, *123*, 1–102; c) S. Kodani, J. Bicz, L. Song, R. J. Deeth, M. Ohnishi-Kameyama, M. Yoshida, K. Ochi, G. L. Challis, *Org. Biomol. Chem.* **2013**, *11*, 4686–4694.
[2] a) C. J. Carrano, M. Jordan, H. Drechsel, D. G. Schmid, G. Winkelmann, *BioMetals* **2001**, *14*, 119–125; b) M. Sritharan, *J. Bacteriol.* **2016**, *198*, 2399–2409.
[3] S. Dunghana, M. J. Miller, L. Dong, C. Ratledge, A. L. Crumbliss, *J. Am. Chem. Soc.* **2003**, *125*, 7654–7663.
[4] P. R. Sridhar, B. C. Venkatesh, S. Kalesha, C. Sudharani, *Org. Biomol. Chem.* **2018**, *16*, 3732–3740.
[5] a) C. Kurth, H. Kage, M. Nett, *Org. Biomol. Chem.* **2016**, *14*, 8212–8227; b) I. J. Schalk, *J. Med. Chem.* **2018**, *61*, 3842–3844.
[6] a) N. von Wirén, S. Klair, S. Bansal, J.-F. Briat, H. Khodr, T. Shioiri, R. A. Leigh, R. C. Hider, *Plant Physiol.* **1999**, *119*, 1107–1114.
[7] a) R. Hermenau, K. Ishida, S. Gama, B. Hoffmann, M. Pfeifer-Leeg, W. Plass, J. F. Mohr, T. Wichard, H.-P. Saluz, C. Hertweck, *Nat. Chem. Biol.* **2018**, *14*, 841–843; b) C. Makris, J. R. Carmichael, H. Zhou, A. Butler, *ACS Chem. Biol.* **2022**, *17*, 3140–3147.
[8] G. J. Sharman, D. H. Williams, D. F. Ewing, C. Ratledge, *Chem. Biol.* **1995**, *2*, 553–561.
[9] L. Dong, M. J. Miller, *J. Org. Chem.* **2002**, *67*, 4759–4760.
[10] A. Sornosa-Ten, P. Jewula, T. Fodor, S. Brandès, V. Sladkov, Y. Rousselin, C. Stern, J.-C. Chambron, M. Meyer, *New J. Chem.* **2018**, *42*, 7765–7779.
[11] a) K. N. Raymond, S. S. Isied, L. D. Brown, F. R. Fronczek, J. H. Nibert, *J. Am. Chem. Soc.* **1976**, *98*, 1767–1774; b) B. F. Anderson, D. A. Buckingham, G. B. Robertson, J. Webb, K. S. Murry, P. E. Clark, *Nature* **1976**, *262*, 722–724; c) T. B. Karpishin, M. S. Gebhard, E. I. Solomon, K. N. Raymond, *Inorg. Chem.* **1991**, *113*, 2977–2984; d) S. L. Jewett, S. Eggling, L. Geller, *J. Inorg. Biochem.* **1997**, *66*, 165–173; e) M. J. Sever, J. J. Wilker, *Dalton Trans.* **2004**, *n/a*, 1061–1072.
[12] a) D. A. Brown, D. McKeith (née Byrne), W. K. Glass, *Inorg. Chim. Acta* **1979**, *35*, 5–10; b) B. Monzyk, A. L. Crumbliss, *J. Inorg. Biochem.* **1983**, *19*, 19–39; c) J. O. M. Herrera, L. Coelho Paes, A. M. Canavarro Benites, R. Marchiori, S. P. Machado, B. C. Machado, *Quim. Nova* **2006**, *29*, 269–276; d) T. Terencio, J. Roithová, S. Brandès, Y. Rousselin, M.-J. Penouilh, M. Meyer, *Inorg. Chem.* **2018**, *57*, 1125–1135.
[13] a) L. Panizzi, G. Di Maio, P. A. Tardella, L. d'Abbiero, *Ric. Sci.* **1961**, *1(IIA)*, 310–313; b) Societa Farmaceutici Italia. Saturated *N*-hydroxylactams. Patent 955.945, **1964**; c) S. M. Neset, T. Bennecher, K. Undheim, *Acta Chem. Scand.* **1993**, *47*, 1141–1143; d) R. Banerjee, S. B. King, *Org. Lett.* **2009**, *11*, 4580–4583.
[14] a) S. A. Matlin, P. G. Sammes, *J. Chem. Soc., Chem. Commun.* **1972**, *n/a*, 1222–1223; b) S. A. Matlin, P. G. Sammes, R. M. Upton, *J. Chem. Soc., Perkin Trans. 1* **1979**, *n/a*, 2481–2487; c) A. Drouin, D. K. Winter, S. Pichette, S. Aubert-Nicol, J. Lessard, C. Spino, *J. Org. Chem.* **2011**, *76*, 164–169.
[15] P. Jewula, J.-C. Berthet, J.-C. Chambron, Y. Rousselin, P. Thuéry, M. Meyer, *Eur. J. Inorg. Chem.* **2015**, *n/a*, 1529–1541.
[16] P. Jewula, J.-C. Chambron, M.-J. Penouilh, Y. Rousselin, M. Meyer, *RSC Adv.* **2014**, *4*, 22743–22754.
[17] R. Raavé, G. Sandker, P. Adumeau, C. B. Jacobsen, F. Mangin, M. Meyer, M. Moreau, C. Bernhard, L. Da Costa, A. Dubois, V. Goncalves, M. Gustaffson, M. Rijpkema, O. Boerman, J.-C. Chambron, S. Heskamp, F. Denat, *Eur. J. Nucl. Med. Mol. Imaging* **2019**, *46*, 1966–1977.
[18] N. Kircheva, T. Dudev, *Inorg. Chem.* **2020**, *59*, 6242–6254.
[19] F. C. Bradley, C. M. Giandomenico, M. J. Abrams, D. T. Frost, J. F. Vollano, European patent application 92301851.9, **1992**.
[20] S. Brandès, A. Sornosa-Ten, Y. Rousselin, M. Lagrelette, C. Stern, A. Moncomble, J.-P. Cornard, M. Meyer, *J. Inorg. Biochem.* **2015**, *151*, 164–175.
[21] J. Yang, P. J. Bremer, I. L. Lamont, A. J. McQuillan, *Langmuir* **2006**, *22*, 10109–10117.
[22] J. C. Bailar, *J. Inorg. Nucl. Chem.* **1958**, *8*, 165–175.
[23] P. C. Rây, N. K. Dutt, *J. Indian Chem. Soc.* **1943**, *20*, 81.
[24] B. Kersting, J. R. Telford, M. Meyer, K. N. Raymond, *J. Am. Chem. Soc.* **1996**, *118*, 5712–5721.
[25] A. Rodger, B. F. G. Johnson, *Inorg. Chem.* **1988**, *27*, 3061–3062.
[26] S. S. Eaton, G. R. Eaton, R. H. Holm, E. L. Muetterties, *J. Am. Chem. Soc.* **1973**, *95*, 1116–1124.
[27] M. Pinsky, D. Avnir, *Inorg. Chem.* **1998**, *37*, 5575–5582.
[28] S. Alvarez, D. Avnir, M. Llunell, M. Pinsky, *New J. Chem.* **2002**, *26*, 996–1009.
[29] S. Alvarez, P. Alemany, D. Casanova, J. Cirera, M. Llunell, D. Avnir, *Coord. Chem. Rev.* **2005**, *249*, 1693–1708.
[30] J. Cirera, E. Ruiz, S. Alvarez, *Organometallics* **2005**, *24*, 1556–1562.
[31] K. R. Dymok, G. J. Palenik, *Inorg. Chem.* **1975**, *14*, 1220–1222.
[32] D. L. Kepert, *Prog. Inorg. Chem.* **1977**, *23*, 1–65.
[33] M. R. Seyedsayamdost, M. F. Traxler, S.-L. Zheng, R. Kolter, J. Clardy, *J. Am. Chem. Soc.* **2011**, *133*, 11434–11437.

Manuscript received: January 20, 2023
Revised manuscript received: February 20, 2023